NASA Contractor Report 185215

Aperture Taper Determination for the Half-Scale Accurate Antenna Reflector

Kevin M. Lambert
Analex Corporation
NASA Lewis Research Center
Cleveland, Ohio

April 1990

Prepared for
Lewis Research Center
Under Contract NAS3-24564

National Aeronautics and
Space Administration

APERTURE TAPER DETERMINATION FOR THE HALF-SCALE ACCURATE ANTENNA REFLECTOR

Kevin M. Lambert
Analex Corporation
NASA Lewis Research Center
Cleveland, Ohio 44135

SUMMARY

This report describes a simulation of a proposed microwave reflectance measurement in which the half scale reflector is used in a compact range type of application. The simulation is used to determine an acceptable aperture taper for the reflector which will allow for accurate measurements. Information on the taper is used in the design of a feed for the reflector.

INTRODUCTION

An earlier report (ref. 1) studied the computed performance of the half-scale, accurate antenna reflector (ref. 2). In the report, the reflector was evaluated with respect to its ability to generate a nearfield, plane wave for a compact range application. The report concluded that an aperture taper of -30 dB was necessary in order to achieve a quiet zone with a desirable ripple performance. The desirable level of amplitude ripple was considered to be 0.1 dB which has been shown to be a requirement for sensitive measurements (ref. 3). The report also showed that although the quiet zone was small because of the high taper, it was of sufficient size to measure the anticipated test articles. This report however did not address the problem of designing a reflector feed that would allow this performance to be achieved.

An investigation was conducted to find a design of a corrugated horn antenna that would deliver the desired performance. Corrugated horns were considered because this type of horn produces a beam with circular symmetry which holds over a substantial bandwidth. The investigation showed that a roughly seven wavelength aperture, containing only the HE_{11} mode of a corrugated waveguide, would produce the -30 dB taper on the reflector. However, a suitable transition from conventional waveguide to a corrugated waveguide of such a large diameter could not be found. Several types of transitions were modeled but each type generated enough HE_{12} mode in the aperture so as to corrupt the pattern. The HE_{12} mode broadened the main beam which prevented the -30 dB taper from being achieved.

Since the desired taper cannot be realized, the ripple requirement in the quiet zone, and hence the taper requirement, will have to be relaxed. The effect that this may have on the anticipated measurements is the subject of this report. Here, a two-dimensional model of the experiment is developed. The model is used to compare the desired measured response of the test object with the corrupting error response that is present due to the diffractions at the edges of the reflector. This comparison reveals the amount of taper that is necessary in order to keep the error response insignificant. Information obtained from this simulation is used as a guide in the design of a corrugated horn feed for the reflector.

The report begins with a description of the response of the test object due to an incident plane wave. This response is then used as the field incident on the reflector. The reflected field and the diffracted field are calculated at the focus of the reflector. Since the reflected field is the desired field and the diffracted field causes the measurement error, the two are compared over the frequency range of interest.

NEARFIELD BISTATIC SCATTERING FROM A TWO-DIMENSIONAL STRIP

The anticipated test articles that will be used in the measurements are plates. Therefore, this two-dimensional model of the experiment must calculate the nearfield bistatic scattering from a strip. The geometry for this calculation is shown in figure 1. The strip is of width d and is infinite in the $\hat{z}$ direction. A $\hat{z}$ polarized plane wave is assumed to be incident from the $-\hat{x}$ direction. The goal is to find the scattered field as a function of ϕ for $0° \leq \phi \leq 90°$. Note that the scattering will be symmetric about $\phi = 0°$. Geometrical optics and the Uniform Theory of Diffraction (UTD) (ref. 4) will be used to calculate the scattering. Only first order scattering is considered.

The field incident on the strip is written as,

$$\bar{E}^i = -E_o e^{jkx}\,\hat{z} \tag{1}$$

where $k = 2\pi/\lambda$ and E_o is a constant. The form of the field depends on which region the observation point is in. Referring to figure 1, the regions are defined by,

$$\text{Region I} \qquad \rho \sin\phi \leq d/2 \tag{2}$$

$$\text{Region II} \qquad \rho \sin\phi \geq d \tag{3}$$

with the boundary being the reflection shadow boundary. In Region I, the scattered field consists of three terms, the reflected field and the diffracted field at each edge. The field in this region can be written as,

$$\bar{E}^t = \bar{E}^R + \bar{E}^d_1 + \bar{E}^d_2 \qquad [\text{Region I}] \tag{4}$$

where $\bar{E}^t$ is the total field, $\bar{E}^R$ is the reflected field and $\bar{E}^d_i$ is the field diffracted from edge i. The edges are numbered in figure 1. The reflected field is simply,

$$\bar{E}^R = E_o e^{-jkx}\,\hat{z}\ . \tag{5}$$

Using UTD, the diffracted field from an edge is,

$$\bar{E}^d_i = -E_o D_{si}\,\frac{e^{-jk\rho_i}}{\sqrt{\rho_i}}\,\hat{z}\ . \tag{6}$$

Here, D_{si} is the soft scalar diffraction coefficient for edge i and ρ_i is the distance from the edge to the observation point. For the strip, the wedge angle is zero and with plane wave incidence, the diffraction coefficient is given by,

$$D_{si} = D\left(\rho_i, \theta_i - \frac{\pi}{2}\right) - D\left(\rho_i, \theta_i + \frac{\pi}{2}\right) \tag{7}$$

where

$$D(L,\beta) = \frac{-e^{-j\pi/4}}{2\sqrt{2\pi k}} \frac{F[kLa(\beta)]}{\cos(\beta/2)} \tag{8}$$

and

$$a(\beta) = 2\cos^2\left(\frac{\beta}{2}\right) . \tag{9}$$

The function $F[kLa(\beta)]$ is the transition function which is defined in reference 4. The angle for each edge is shown in figure 1.

The remainder of the solution for Region I depends only on geometric considerations. If the observation point is to be described by the cylindrical coordinates (ρ,ϕ), then ρ_i and ϕ_i must be related to them. Using figure 2 and the Law of Cosines, it can be shown that for edge 1,

$$\rho_1 = \sqrt{\rho^2 + \left(\frac{d}{2}\right)^2 - \rho d \sin(\phi)} . \tag{10}$$

Also,

$$\theta_1 = \frac{\pi}{2} + \phi - \alpha \tag{11}$$

where

$$\sin(\alpha) = \frac{d\cos\phi}{2\rho_1} \tag{12}$$

which is found using the Law of Sines. For edge 2, figure 3 is used. Here,

$$\rho_2 = \sqrt{\rho^2 + \left(\frac{d}{2}\right)^2 + \rho d \sin(\phi)} \tag{13}$$

and

$$\phi_2 = \frac{\pi}{2} - \gamma - \phi \tag{14}$$

with

$$\sin(\gamma) = \frac{d\cos\phi}{2} . \tag{15}$$

For Region II, there is no reflected field and the total scattered field is given by the sum of the diffracted fields,

$$\bar{E}^t = \bar{E}_1^d + \bar{E}_2^d \qquad \text{[Region II]} \tag{16}$$

where the diffracted fields are the same as defined above.

A computer program was written, based on the above formulation, to generate the scattering of the strip. Figure 4 presents the magnitude of the scattered field of a 10 in. strip at 10 GHz. The field is shown as function of a constant range ρ = 10 in. Figure 5 shows the scattering for ρ = 100 in. and figure 6 is at the range ρ = 1000 in. In figure 6, the field points are well in the farfield of the strip and the scattering exhibits the familiar sin(x)/x behavior as expected.

At ρ = 5000 in. the monostatic echo width of the strip,

$$\sigma = 2\pi\rho \left| \frac{E^t}{E_o} \right|^2 \tag{17}$$

is calculated to be 11.24 dB above a square meter (dBsm). Noting that the theoretical echo width is 11.31 dBsm, the program appears to calculate the scattering correctly. The program is used to calculate the scattered field that is incident on the reflector. The modeling of the scattering by the reflector is described in the following section.

NEARFIELD SCATTERING FROM AN OFFSET, PARABOLIC CYLINDER

The scattering by an offset, parabolic cylinder may be developed by assuming the incident field originates from two electric line sources and a plane wave confined to Region I. This situation is depicted in figure 7. Here, the electric line sources represent the scattering from the edges of the strip. The plane wave in Region I is the Geometrical Optics (GO) field reflected by the strip. Once the general solution is found using these sources, the specific solution can be found by including the results of the previous section.

The intent of this section is to find the scattered field of the parabolic cylinder, at the focus of the cylinder. The scattered field is generated by two mechanisms. The first is the field reflected by the reflector. The second is the fields scattered by the edges of the reflector. These fields are undesired and result in measurement error when present at the focus. The goal of this analysis is to determine the magnitude of the error. This analysis will not include direct scattering by the strip to the focal point. The error fields will be considered first.

As in the two-dimensional strip scattering analysis, the UTD formulation for edge diffraction will be used to find the diffracted fields. Thus, the solution is essentially an exercise in geometry. Figure 8 introduces the variables used in the development of the solution. The reflector has a width of D, an offset height of h, and a focal length, f. The electric line sources, representing the edges of the strip, are separated by the distance d and are centered a height H above the axis of the parabola. The line sources are a distance R from the vertex of the parabola.

The first step in the solution is to define the location of the line sources and the reflector edges. The origin of the coordinate system is the vertex of the parabola. The respective sources and edges are defined in figure 8. Their coordinates are given by,

$$\left.\begin{aligned}
(x_0,y_0) &= (R,H) \\
(x_1,y_1) &= \left(R,\ H + \frac{d}{2}\right) \\
(x_2,y_2) &= \left(R,\ H - \frac{d}{2}\right) \\
(x_3,y_3) &= \left(\frac{y_3^2}{4f},\ h + D\right) \\
(x_4,y_4) &= \left(\frac{y_4^2}{4f},\ h\right)
\end{aligned}\right\} \tag{18}$$

where the equation of the parabola is used for the location of edges 3 and 4.

The distances between the line sources and the reflector edges, and between the reflector edges and the focus need to be known. The individual distances are defined in figure 8 and they are given by,

$$\left.\begin{aligned}
\rho_{13} &= \sqrt{(x_1 - x_3)^2 + (y_3 - y_1)^2} & \rho_{14} &= \sqrt{(x_1 - x_4)^2 + (y_1 - y_4)^2} \\
\rho_{23} &= \sqrt{(x_2 - x_3)^2 + (y_3 - y_2)^2} & \rho_{24} &= \sqrt{(x_2 - x_4)^2 + (y_2 - y_4)^2} \\
\rho_3 &= \sqrt{(f - x_3)^2 + y_3^2} & \rho_4 &= \sqrt{(f - x_4)^2 + y_4^2}\ .
\end{aligned}\right\} \tag{19}$$

Further, to compute the diffracted field from the reflector edges, the angles between the reflector surface tangent and the incident rays and the angle between the surface tangent and the ray to the focus must be determined. These angles are defined in figure 9 as well as figure 8. The angles to the observation point are given by,

$$\theta_3 = \frac{\pi}{2} - \frac{\alpha_3}{2} \tag{20}$$

$$\theta_4 = \frac{\pi}{2} + \frac{\alpha_4}{2} \tag{21}$$

where,

$$\alpha_3 = 2 \tan^{-1}\left(\frac{y_3}{4f}\right) \tag{23}$$

and

$$\alpha_4 = 2 \tan^{-1}\left(\frac{y_4}{4f}\right) . \tag{24}$$

The angles to the incident rays are given by,

$$\left.\begin{aligned} \phi_{13} &= \theta_3 + \cos^{-1}\left(\hat{\rho}_{13} \cdot \hat{\rho}_3\right) \\ \phi_{23} &= \theta_3 + \cos^{-1}\left(\hat{\rho}_{23} \cdot \hat{\rho}_3\right) \\ \phi_{14} &= \theta_4 - \cos^{-1}\left(\hat{\rho}_{14} \cdot \hat{\rho}_4\right) \\ \phi_{24} &= \theta_4 - \cos^{-1}\left(\hat{\rho}_{24} \cdot \hat{\rho}_4\right) \end{aligned}\right\} \tag{25}$$

where the unit vectors are defined by,

$$\left.\begin{aligned} \hat{\rho}_{13} &= \frac{\bar{\rho}_{13}}{\rho_{13}} \qquad \hat{\rho}_{14} = \frac{\bar{\rho}_{14}}{\rho_{14}} \qquad \hat{\rho}_3 = \frac{\bar{\rho}_3}{\rho_3} \\ \hat{\rho}_{23} &= \frac{\bar{\rho}_{23}}{\rho_{23}} \qquad \hat{\rho}_{24} = \frac{\bar{\rho}_{24}}{\rho_{24}} \qquad \hat{\rho}_4 = \frac{\bar{\rho}_4}{\rho_4} \end{aligned}\right\} \tag{26}$$

with the incident vectors being,

$$\left.\begin{aligned} \bar{\rho}_{13} &= (x_1 - x_3)\hat{x} + (y_1 - y_3)\hat{y} \qquad \bar{\rho}_{14} = (x_1 - x_4)\hat{x} + (y_1 - y_4)\hat{y} \\ \bar{\rho}_{23} &= (x_2 - x_3)\hat{x} + (y_2 - y_3)\hat{y} \qquad \bar{\rho}_{24} = (x_2 - x_4)\hat{x} + (y_2 - y_4)\hat{y} \\ \bar{\rho}_3 &= (f - x_3)\hat{x} + (-y_3)\hat{y} \qquad \bar{\rho}_4 = (f - x_4)\hat{x} + (-y_4)\hat{y} . \end{aligned}\right\} \tag{27}$$

With all of the geometric parameters defined, and expression for the edge diffracted field at the focus may be written as,

$$\bar{E}_d^f = \left(E_d^{31} + E_d^{32} + E_d^{41} + E_d^{42}\right)\hat{z} \tag{28}$$

where E_d^{ij} implies the field diffracted from edge i with incident field from source j. Using the UTD formulation, these fields are given by,

$$E_d^{31} = E_i^{31} \frac{e^{-jk\rho_3}}{\sqrt{\rho_3}} \left[D\left(\frac{\rho_{13}\rho_3}{\rho_{13}+\rho_3}, \theta_3 - \phi_{13} \right) - D\left(\frac{\rho_{13}\rho_3}{\rho_{13}+\rho_3}, \theta_3 + \phi_{13} \right) \right] \tag{29}$$

$$E_d^{32} = E_i^{32} \frac{e^{-jk\rho_3}}{\sqrt{\rho_3}} \left[D\left(\frac{\rho_{23}\rho_3}{\rho_{23}+\rho_3}, \theta_3 - \phi_{23} \right) - D\left(\frac{\rho_{23}\rho_3}{\rho_{23}+\rho_3}, \theta_3 + \phi_{23} \right) \right] \tag{30}$$

$$E_d^{41} = E_i^{41} \frac{e^{-jk\rho_4}}{\sqrt{\rho_4}} \left[D\left(\frac{\rho_{14}\rho_4}{\rho_{14}+\rho_4}, \theta_4 - \phi_{14} \right) - D\left(\frac{\rho_{14}\rho_4}{\rho_{14}+\rho_4}, \theta_4 + \phi_{14} \right) \right] \tag{31}$$

$$E_d^{42} = E_i^{42} \frac{e^{-jk\rho_4}}{\sqrt{\rho_4}} \left[D\left(\frac{\rho_{24}\rho_4}{\rho_{24}+\rho_4}, \theta_4 - \phi_{24} \right) - D\left(\frac{\rho_{24}\rho_4}{\rho_{24}+\rho_4}, \theta_4 + \phi_{24} \right) \right] . \tag{32}$$

Here, the diffraction coefficient used in equation (8) is used. Also, E_i^{nm} is the incident field on edge n from source m. The analysis of the previous section is used to compute this incident field.

To compute the reflected field at the focus, both the electric line sources, representing the strip edges, and the plane wave field of the GO scattering must be considered. To compute the reflected field due to the lines sources, consider figure 10. Here, the line sources are at (x_1,y_1) and (x_2,y_2) as before. The point (x_5,y_5) is the reflection point on the reflector for the line source at (x_1,y_1). The point (x_6,y_6) is the reflection point for the line source at (x_2,y_2). The reflection points are given by,

$$\begin{aligned} (x_5,y_5) &= \left(\frac{y_5^2}{4f}, H + \frac{d}{2} \right) \\ (x_6,y_6) &= \left(\frac{y_6^2}{4f}, H - \frac{d}{2} \right) . \end{aligned} \tag{33}$$

The distance between the line sources and the reflection points are given by,

$$\begin{aligned} \rho_{15} &= R - x_5 \\ \rho_{26} &= R - x_6 . \end{aligned} \tag{34}$$

The distances between the reflection points and the focus are,

$$\left.\begin{aligned} \rho_5 &= \sqrt{(f - x_5)^2 + y_5^2} \\ \rho_6 &= \sqrt{(f - x_6)^2 + y_6^2} \end{aligned}\right\}. \tag{35}$$

The angles defined in figure 10 are given by

$$\left.\begin{aligned} \alpha_5 &= 2 \tan^{-1}\left(\frac{x_5}{2f}\right) \\ \alpha_6 &= 2 \tan^{-1}\left(\frac{x_6}{2f}\right) \end{aligned}\right\} \tag{36}$$

and

$$\left.\begin{aligned} \theta_5 &= \frac{\alpha_5}{2} \\ \theta_6 &= \frac{\alpha_6}{2} \end{aligned}\right\}. \tag{37}$$

To compute the reflected field, the radius of curvature of the reflector must be known at the reflection point. The general form of the radius of curvature for a parabola is shown in the appendix. Using the result shown there, the radius of curvature at point five is given by,

$$R_g^5 = \frac{2(x_5 + f)^{3/2}}{\sqrt{f}} \tag{38}$$

and for point six

$$R_g^6 = \frac{2(x_6 + f)^{3/2}}{\sqrt{f}} . \tag{39}$$

The radii of curvature are used to find the reflected field caustics. The general equation for a reflected field caustic is given by,

$$\frac{1}{\rho^r} = \frac{1}{\ell_i} + \frac{2}{R_g \cos(\theta)}$$

where ρ^r is the caustic distance, ℓ_i is the distance between the source and reflection point and θ is the angle between the surface normal and the direction of the incoming field. Thus, for this particular problem,

$$\frac{1}{\rho_5^r} = \frac{1}{\rho_{15}} + \frac{2}{R_g^5 \cos(\theta_5)} \tag{40}$$

and

$$\frac{1}{\rho_6^r} = \frac{1}{\rho_{16}} + \frac{2}{R_g^6 \cos(\theta_6)} \ . \tag{41}$$

The total reflected field, at the focus, from the incident field of the line sources is written as,

$$\bar{E}^f_{R,d} = \left(E_R^{51} + E_R^{61}\right)\hat{z} \tag{42}$$

where E_R^{ij} implies the reflected field at point i due to the field from source j. These fields are given by,

$$E_R^{51} = -E_i^{51}\sqrt{\frac{\rho_5^r}{\rho_5^r + \rho_5}}\, e^{-jk\rho_5} \tag{43}$$

$$E_R^{62} = -E_i^{62}\sqrt{\frac{\rho_6^r}{\rho_6^r + \rho_6}}\, e^{-jk\rho_6} \ . \tag{44}$$

E_i^{51} and E_i^{61} are the incident fields at the reflection points. The analysis of the previous section is used to find the incident fields.

To find the reflected field at the focus that is due to the GO scattering of the strip, a Physical Optics (PO) integration must be done over the surface of the reflector. Consider the geometry shown in figure 11. The GO field is confined to Region I or $y_6 \leq y \leq y_5$. This field is written as,

$$\bar{E}^i_R = E_o e^{-jkx}\,\hat{z} \qquad H - \frac{d}{2} \leq y \leq H + \frac{d}{2} \tag{45}$$

which is from equation (5). The plane of the strip is taken as a reference plane and hence ρ'' is the distance between the plane and a point on the reflector. The distance ρ' is between the same point on the reflector and the focus. From the properties of the parabola, the sum of these distances is a constant,

$$\rho' + \rho'' = C$$

where

$$C = f + R$$

Since

$$\rho' = \frac{4f^2 + y^2}{4f} = f$$

it can be found that,

$$\rho'' = R - x' \tag{46}$$

where x' is shown in figure 11.

Using the PO approximation, the surface current on the reflector is given by,

$$\bar{J}_s = 2\hat{n} \times \bar{H}_R^i \tag{47}$$

where $\bar{H}_R^i$ is the incident magnetic field and $\hat{n}$ is the surface normal. Using equation (45) and the plane wave relationship between the electric and magnetic field, the magnetic field is written as,

$$\bar{H}_R^i = \frac{-E_o}{\eta} e^{-jkx} \hat{y} \tag{48}$$

where η is the impedance of free space. Using equations (46), (47) and (48), and the expression for the normal found in the appendix, the surface current is found to be,

$$\bar{J}_s = \frac{-2E_o}{\eta} \sqrt{\frac{f}{f + x'}} e^{-jk(R-x')} \hat{z} \ . \tag{49}$$

The two-dimensional radiation integral for a $\hat{z}$ directed current is given by reference 5,

$$E_z = \frac{-k\eta}{4} \int_{\ell} J_z H_o^{(2)}(k\rho) d\ell \tag{50}$$

where $H_o^{(2)}(k\rho)$ is the Hankel function of the second kind and ℓ is the length over which the current is present. From figure 12, it can be found that,

$$d\ell = \frac{dx}{\sin(\theta'/2)}$$

and because

$$\sin^2\left(\frac{\theta'}{2}\right) = 1 - \cos^2\left(\frac{\theta'}{2}\right) = 1 - \frac{f}{\rho'} = \frac{x}{f + x}$$

it can be written,

$$d\ell = \frac{dx}{\sqrt{\frac{x}{f + x}}} \ . \tag{51}$$

Using equations (49) and (51) in equation (50) and substituting $\rho' = \rho$ the reflected field at the focus, from GO incidence is found to be

$$\bar{E}_R^f = -E_o \frac{kf}{2} e^{-jkR} \int_{x_6}^{x_5} H_o^{(2)} \frac{(k(f + x'))}{\sqrt{x'}} e^{jkx'} dx' \hat{z} . \qquad (52)$$

This equation can be integrated numerically.

In summary, there are three contributions to the reflected field at the focus. Two contributions are due to diffractions from the edge of the strip. These contributions are given by equation (42). The second contribution is from the GO return of the strip. This is given by equation (52). The next section will show the results based on this analysis.

EXPERIMENTAL SIMULATION

The geometry of the half scale reflector allows the following parameters to be defined for the two-dimensional simulation, D = 53.40 in., h = 28.06 in., and f = 66.00 in. As an example of a test object, consider a strip with d = 10.00 in. located at twice the focal length of the reflector, R = 132.00 in. The strip is centered in the center of the reflector aperture, thus, H = 54.76 in.

The three components of the scattered field at the focus are shown in figure 13, for a frequency range from 8 to 12 GHz. Figure 13(a) shows E_R^f, figure 13(b) shows $E_{R,d}^f$ and figure 13(c) shows E_d^f. These figures show the magnitude in decibels but the reference level is arbitrary. Scalar notation is used since all fields are polarized in the same direction.

Figure 14 shows a plot of the ratio (in decibels),

$$\frac{E_d^f}{E_R^f + E_{R,d}^f + E_d^f}$$

which is a measure of the level of the error term with respect to the total field at the focus. This plot indicates that the error term is a very small component of the total signal present. Note that these curves are computed assuming there is no aperture taper on the reflector. Thus, uniform illumination of the aperture results in an error term that is roughly -30 dB relative to the GO return.

To see the advantage of allowing some taper on the reflector, consider figure 15 which shows the ratio,

$$\frac{E_d^f}{E_R^f + E_{R,d}^f}$$

which is the ratio between the error term and the ideal term. Two curves are shown, one for a uniform aperture and one for an aperture with -20 dB of taper. Note that the error is reduced by the amount of the taper. This is as expected since the error originates from the edges of the aperture.

To further compare the advantages brought by a taper, consider figure 16 which compares the measured response, with edge diffraction included, to the exact response. Here, no taper is assumed and differences can be seen that are on the order of ±0.25 dB. Figure 17 shows the same comparison except that a -20 dB aperture taper is used. Note that with the taper, there is no discernible difference between the curves.

A -20 dB taper is sufficient to produce an insignificant error term because the desired response of the strip is so large. This taper would not produce an acceptable result for a strip with a smaller backscatter. To demonstrate this, consider a 1 in. strip. Since the length of this strip is one-tenth of the strip in the previous example, E_R^f is -20 dB lower than in the previous example. This is shown in figure 18(a). However, note the plot of $E_{R,d}^f$ in figure 18(b) and E_d^f in figure 18(c). These levels are on the same order as those in the 10 in. example. The net result is that the error is a significant contributor to the total field. This is shown in figure 19 which plots the ratio,

$$\frac{E_d^f}{E_R^f + E_{R,d}^f + E_d^f} .$$

Comparing this curve to figure 14, it is obvious that the performance has been reduced by an amount that is on the order of the reduction of the GO backscatter of the strip. Thus, one could conclude that a -40 dB taper would be required to accurately measure the 1 in. strip.

CONCLUSION

This report has attempted to determine a suitable aperture taper for the half scale reflector during a proposed reflectance measurement. The measurement was modeled in two dimensions using a combination of UTD and PO techniques. The model has provided information on the relative level of the measurement error caused by the diffraction at the edges of the reflector. The error for uniform illumination (no taper) was found to be on the order of -30 dB for an X-Band measurement of a 10 in. strip. Adding taper to the aperture lowers the error by the amount of taper. A calculation was shown for a -20 dB aperture taper. The resulting measurement error was on the order of -50 dB.

With this information, it can be concluded that the original taper requirement of -30 dB can be relaxed significantly for a 10 in. test article. To allow a margin for error, an aperture taper of -20 dB is recommended. A corrugated horn antenna can be designed to produce this taper on the reflector. This recommendation only applies to test articles of this size; however, the margin of error would allow somewhat smaller articles to be tested.

APPENDIX

Consider a parabola defined by the following equation,

$$y^2 = 4fx$$

or

$$y = 2\sqrt{fx}$$

where f is the focal length. The position vector of this parabola is given by,

$$\bar{r} = x\hat{x} + 2\sqrt{fx} \ .$$

The velocity vector is,

$$\bar{r}' = \frac{d\bar{r}}{dx} = \hat{x} + \sqrt{\frac{f}{x}}\,\hat{y}$$

and its derivative is given by,

$$\bar{r}'' = \frac{d^2\bar{r}}{dx^2} = -\frac{1}{2x}\sqrt{\frac{f}{x}}\,\hat{y} \ .$$

The tangent vector is,

$$\hat{t} = \frac{\bar{r}'}{|\bar{r}'|} \frac{\sqrt{x}\,\hat{x} + \sqrt{f}\,\hat{y}}{\sqrt{x + f}} \ .$$

The binormal of the parabola is,

$$\hat{b} = \frac{\bar{r}' \times \bar{r}''}{|\bar{r}' \times \bar{r}''|} = -\hat{z} \ .$$

The normal is given by,

$$\hat{n} = \hat{b} \times \hat{t} = \frac{\sqrt{f}\,\hat{x} - \sqrt{x}\,\hat{y}}{\sqrt{x + f}} \ .$$

The curvature of the parabola is,

$$\kappa = \frac{|\bar{r}' \times \bar{r}''|}{|\bar{r}'|^3} = \frac{\sqrt{f}}{2(x + f)^{3/2}}$$

and the radius of curvature is given by,

$$R = \frac{1}{\kappa} = \frac{2(x + f)^{3/2}}{\sqrt{f}} \ .$$

REFERENCES

1. Lambert, K.M.: Computed Performance of the Half-Scale Accurate Antenna Reflector. NASA CR-182283, 1989.

2. NASA Drawing Numbers: 72076M40A000, 62076M40A100.

3. Burnside, W.D.; and Peters, L. Jr.: Target Illumination Requirements for Low RCS Target Measurements. Evaluation or Aperture Distribution Control to Obtain Improved Compact Range Reflector System Performance. Technical Report. W.D. Burnside and T.H. Lee, Ohio State University, Columbus, OH, 1987, appendix 1.

4. Kouyoumjian, R.G.; and Pathak, P.H.: A Uniform Geometrical Theory of Diffraction for an Edge in a Perfectly Conducting Surface. Proc. IEEE, vol. 62, pp. 1448-1461, Nov. 1974.

5. Harrington, R.F.: Time-Harmonic Electromagnetic Fields. McGraw-Hill, 1961, pp. 228-230.

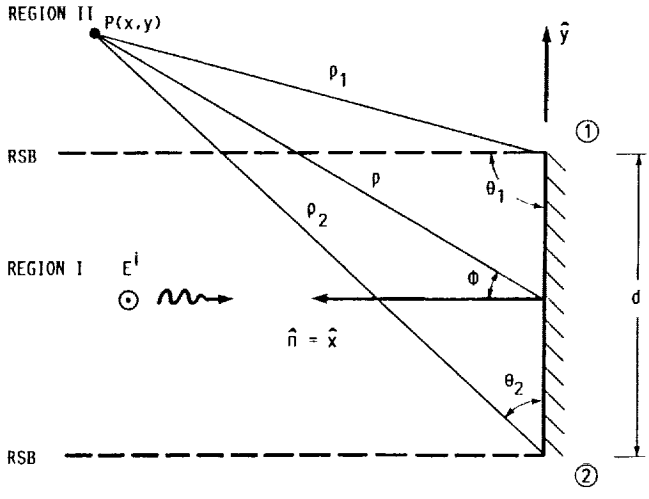

REGION II

FIGURE 1. - GEOMETRY FOR TWO DIMENSIONAL STRIP SCATTERING.

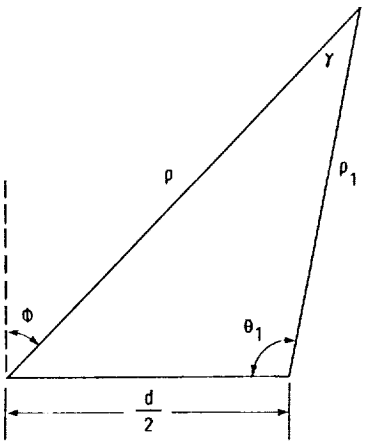

FIGURE 2. - GEOMETRY FOR SCATTERING FROM EDGE 1.

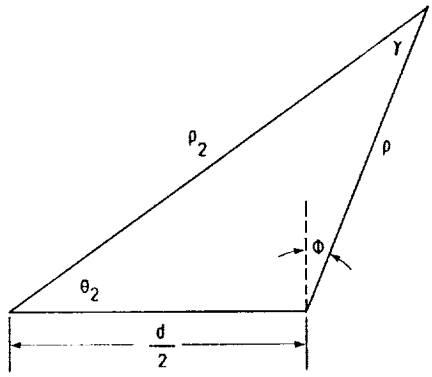

FIGURE 3. - GEOMETRY FOR SCATTERING FROM EDGE 2.

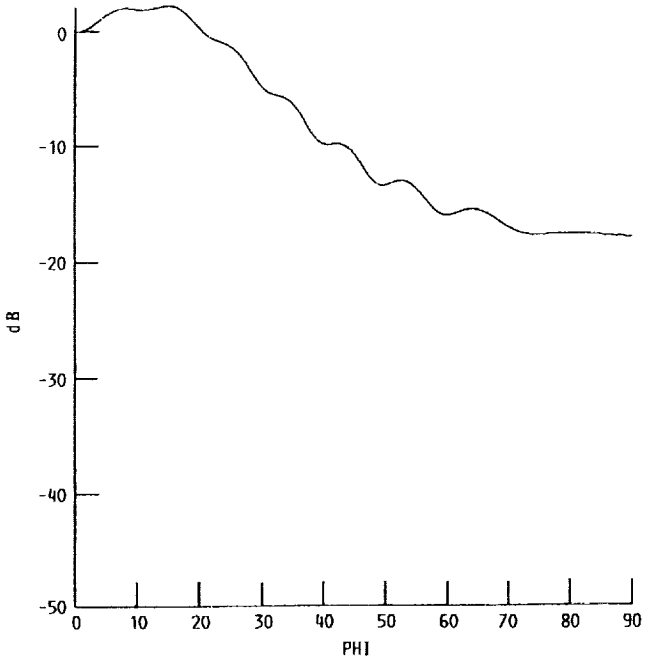

FIGURE 4. - SCATTERED FIELD MAGNITUDE OF A 10 IN. STRIP AT A RANGE OF 10 IN. AND A FREQUENCY OF 10 GHz.

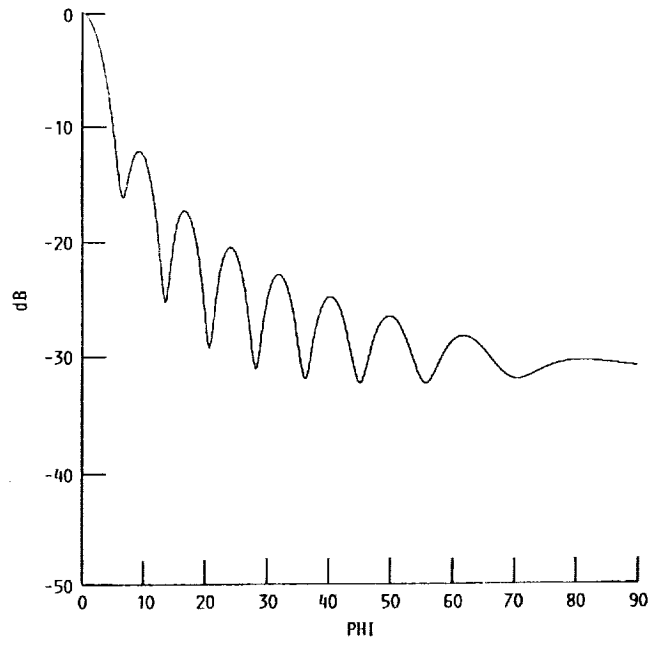

FIGURE 5. - SCATTERED FIELD MAGNITUDE OF A 10 IN. STRIP AT A RANGE OF 100 IN. AND A FREQUENCY OF 10 GHz.

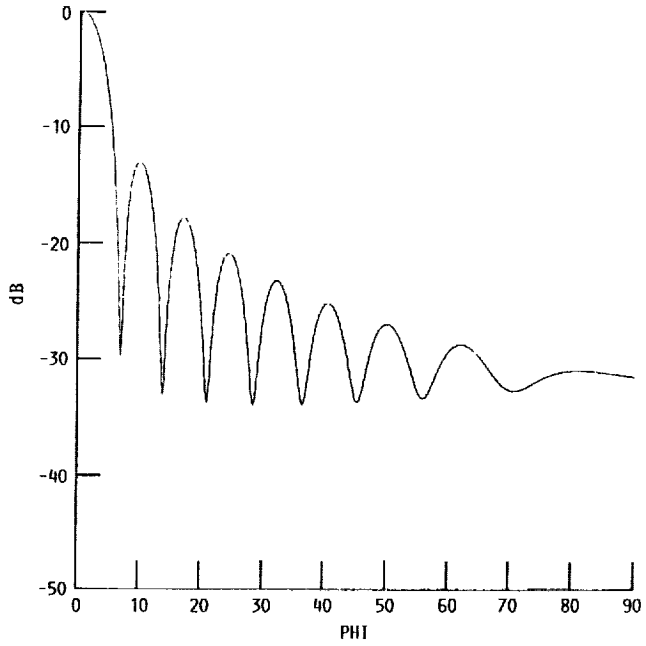

FIGURE 6. - SCATTERED FIELD MAGNITUDE OF A 10 IN. STRIP AT A RANGE OF 1000 IN. AND A FREQUENCY OF 10 GHz.

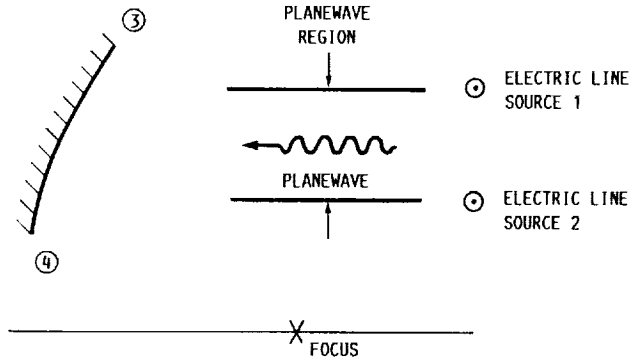

FIGURE 7. - INCIDENT FIELD ON THE PARABOLIC CYLINDER.

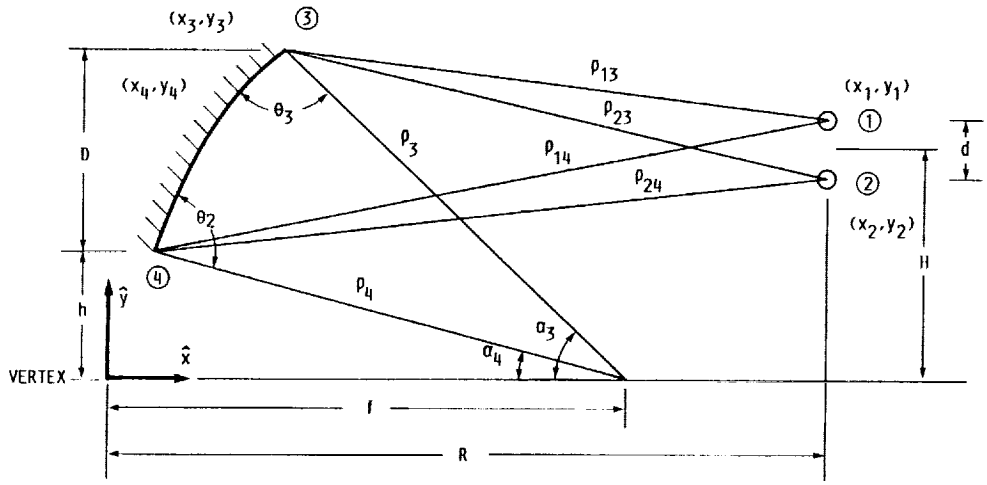

FIGURE 8. - GEOMETRY FOR SCATTERING FROM THE PARABOLIC CYLINDER.

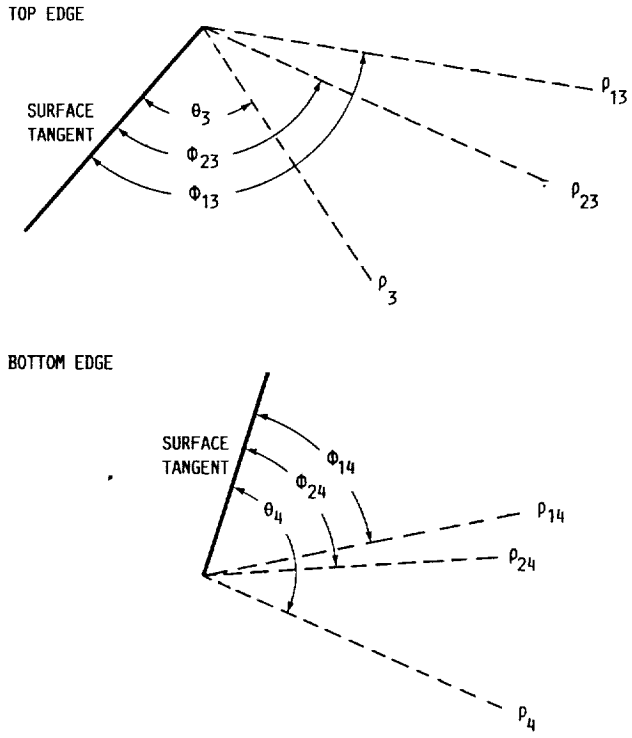

FIGURE 9. - ANGLES FOR SCATTERING FROM THE EDGES OF THE REFLECTOR.

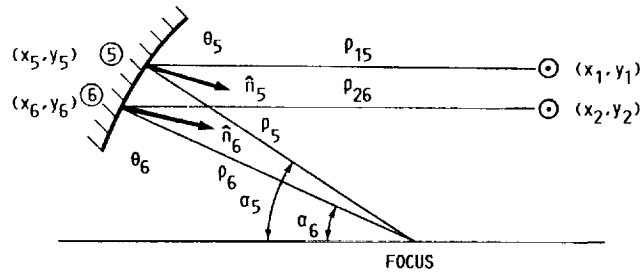

FIGURE 10. - GEOMETRY FOR COMPUTING THE REFLECTED FIELD FROM THE CYLINDER DUE TO THE INCIDENT FIELD OF THE LINE SOURCES.

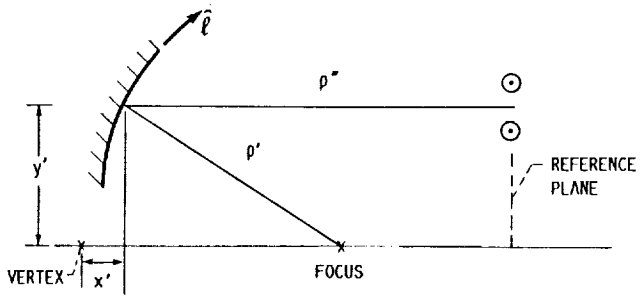

FIGURE 11. - GEOMETRY FOR COMPUTING THE REFLECTED FIELD FROM THE CYLINDER DUE TO THE INCIDENT GO FIELD.

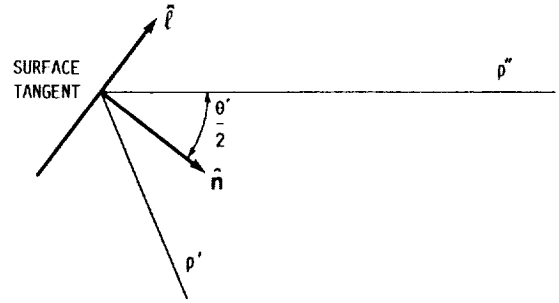

FIGURE 12. - LENGTH ELEMENT FOR PO INTEGRATION.

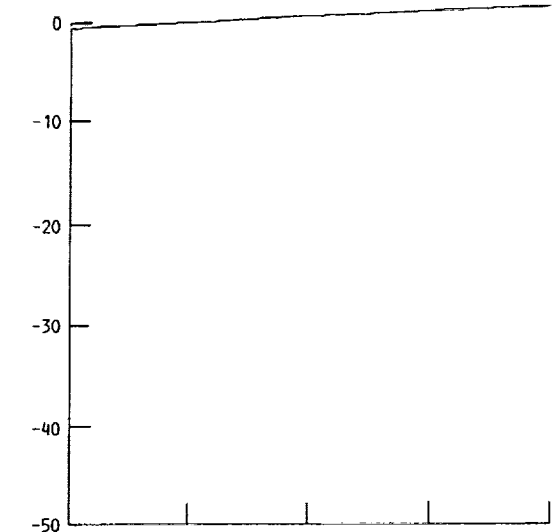

(a) E_R^f.

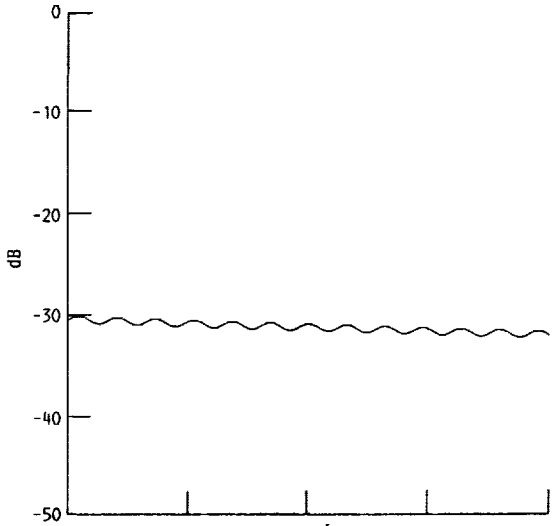

(b) $E_{R,D}^f$.

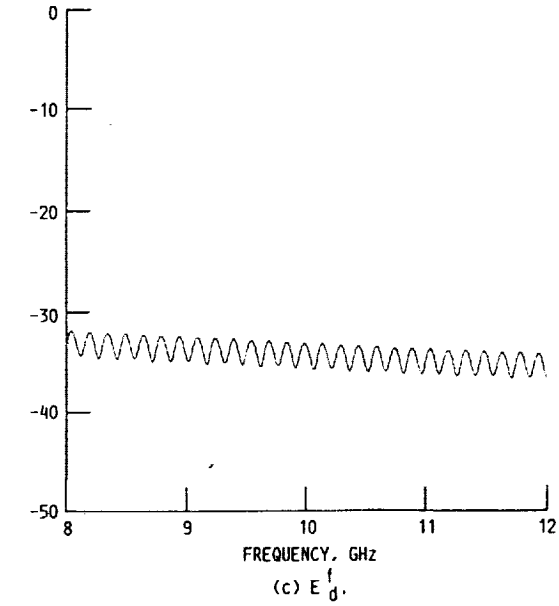

(c) E_d^f.

FIGURE 13. - FIELD TERMS PRESENT AT THE FOCUS OF THE CYLINDER, 10 IN. STRIP AS TEST ARTICLE.

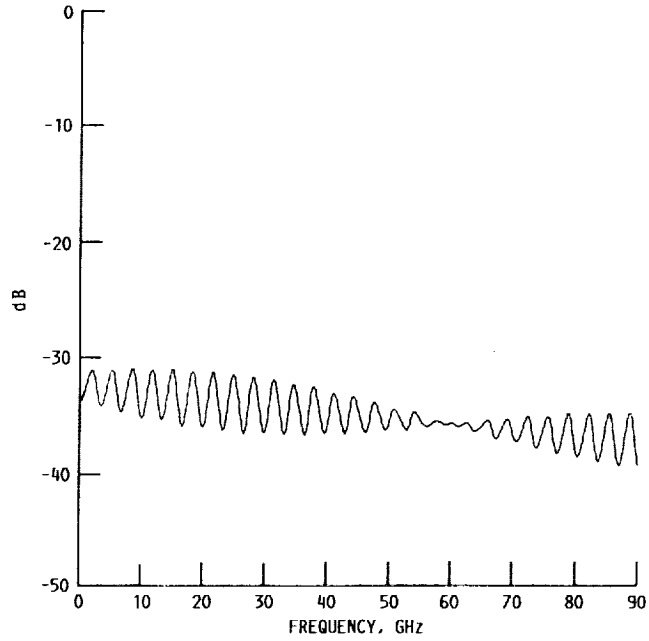

FIGURE 14. - RELATIVE LEVEL OF THE EDGE DEFRACTED TERM TO THE TOTAL FIELD AT THE FOCUS, 10 IN. STRIP.

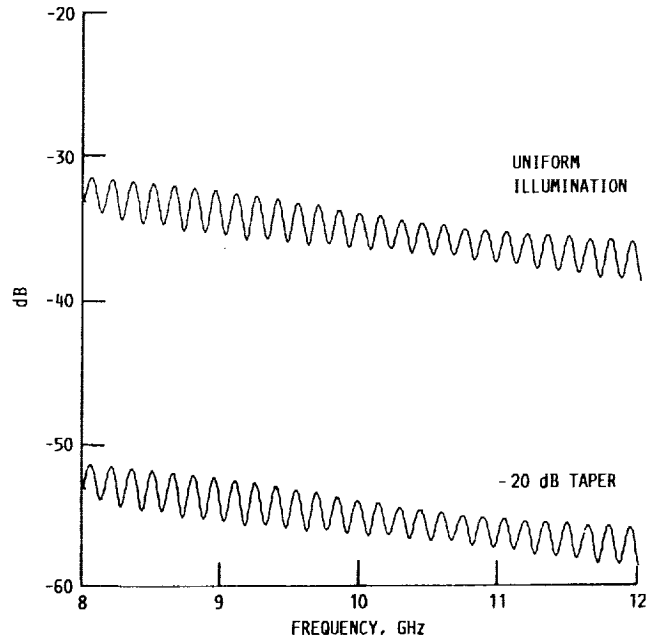

FIGURE 15. - RELATIVE LEVEL OF THE EDGE DIFFRACTION TERM TO THE IDEAL FIELD AT THE FOCUS 10 IN. STRIP.

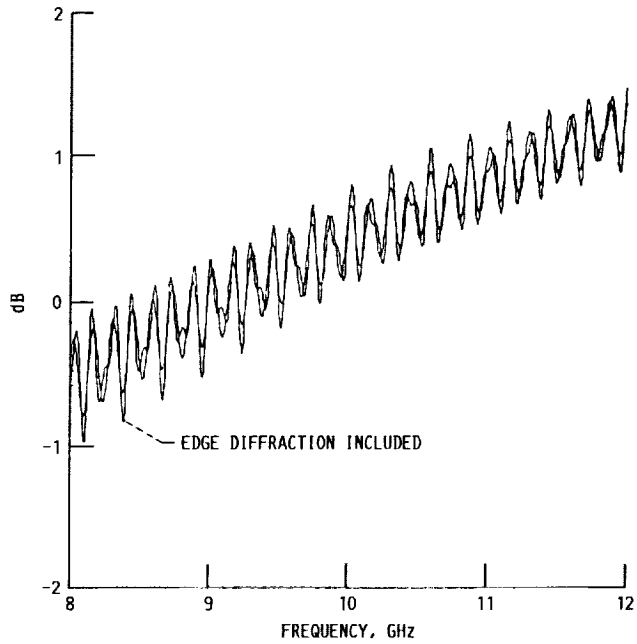

FIGURE 16. - COMPARISON OF THE IDEAL FIELD WITH THE FIELD WITH EDGE DIFFRACTION INCLUDED, 10 IN. STRIP, UNIFORM ILLUMINATION ASSUMED.

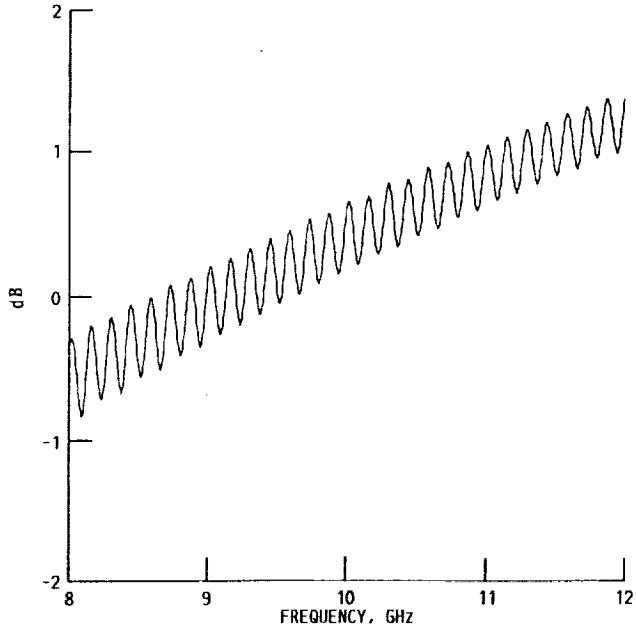

FIGURE 17. - COMPARISON OF THE IDEAL FIELD WITH THE FIELD WITH EDGE DIFFRACTION INCLUDED, 10 IN. STRIP, -20 dB TAPER ASSUMED.

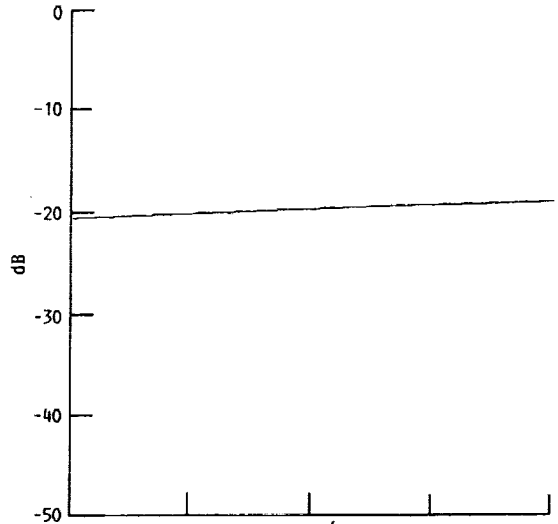

(a) E_R^f.

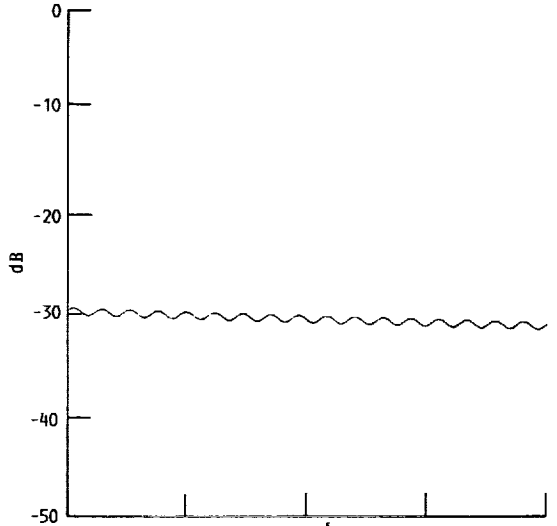

(b) $E_{R,D}^f$.

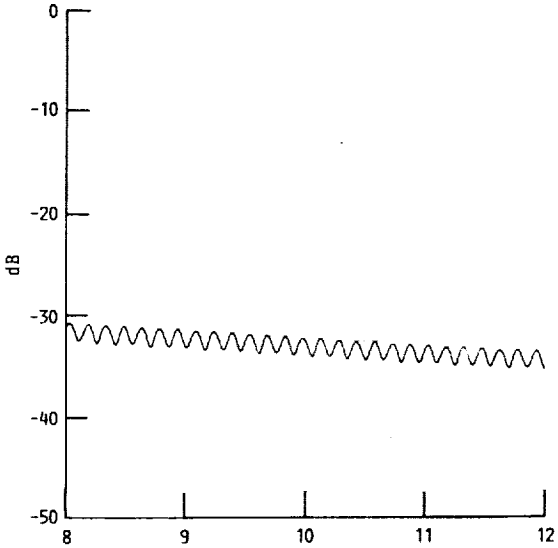

(c) E_d^f.

FIGURE 18. - FIELD TERMS PRESENT AT THE FOCUS OF THE CYLINDER, 1 IN. STRIP AS TEST ARTICLE.

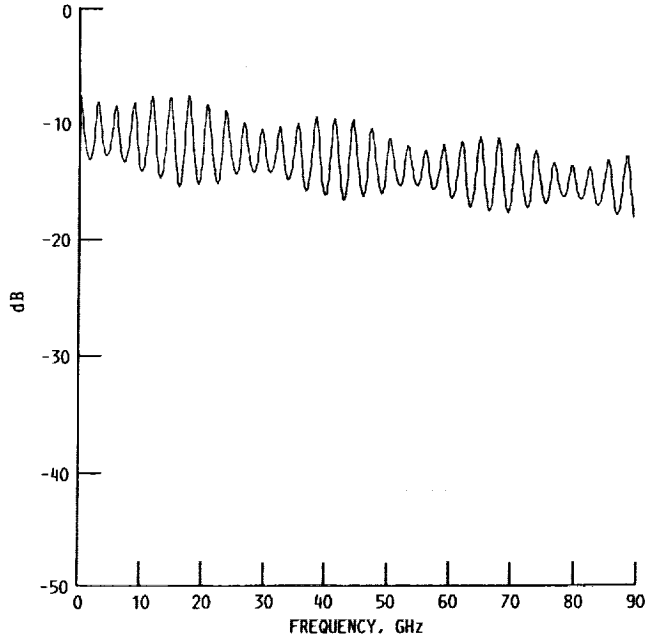

FIGURE 19. - RELATIVE LEVEL OF THE EDGE DIFFRACTED TERM TO THE TOTAL FIELD AT THE FOCUS, 1 IN. STRIP.

NASA
National Aeronautics and Space Administration

Report Documentation Page

1. Report No.	2. Government Accession No.	3. Recipient's Catalog No.
NASA CR-185215		

4. Title and Subtitle	5. Report Date
Aperture Taper Determination for the Half-Scale Accurate Antenna Reflector	April 1990
	6. Performing Organization Code

7. Author(s)	8. Performing Organization Report No.
Kevin M. Lambert	None (E-5373)
	10. Work Unit No.
	650-60-20

9. Performing Organization Name and Address	11. Contract or Grant No.
Analex Corporation NASA Lewis Research Center Cleveland, Ohio 44135	NAS3-24564
	13. Type of Report and Period Covered
	Contractor Report Final
12. Sponsoring Agency Name and Address	14. Sponsoring Agency Code
National Aeronautics and Space Administration Lewis Research Center Cleveland, Ohio 44135-3191	

15. Supplementary Notes

Project Manager, Charles A. Raquet, Space Electronics Division, NASA Lewis Research Center.

16. Abstract

~~This~~ report describes a simulation of a proposed microwave reflectance measurement in which the half scale reflector is used in a compact range type of application. The simulation is used to determine an acceptable aperture taper for the reflector which will allow for accurate measurements. Information on the taper is used in the design of a feed for the reflector.

17. Key Words (Suggested by Author(s))	18. Distribution Statement
Reflector antennas	Unclassified – Unlimited Subject Category 33

19. Security Classif. (of this report)	20. Security Classif. (of this page)	21. No. of pages	22. Price*
Unclassified	Unclassified	22	A03

NASA FORM 1626 OCT 86

*For sale by the National Technical Information Service, Springfield, Virginia 22161